A Two Probes Scanning Phaseless Near-Field Far-Field Transformation Technique

Rocco Pierri, Giuseppe D'Elia, and Francesco Soldovieri

***Abstract*—An innovative and effective technique to determine the far field of a radiating system from near-field intensity data is introduced, analyzed, and tested. The approach is based on the simultaneous measurement of the amplitude of the voltages received by *two* different probe antennas moving over a *single* scanning surface in near zone and performs the phase retrieval of the near field by assuming as unknown the plane wave spectrum of the field. The radiated field is then straightforwardly evaluated. As compared to the existing phaseless measurement techniques, the use of two different probes makes it possible to avoid the need for a second scanning surface and thus allows the use of smaller (and cheaper) anechoic chambers. Furthermore, the measurement time is essentially equal to that required by conventional techniques based on the measurement of the complex near field. The reliability and the effectiveness of the approach are investigated and discussed and the key factors affecting its behavior are highlighted. In particular, the relevance of the difference between the plane wave spectra (PWS) of the two probe antennas in ensuring an acceptable reliability of the solution, with respect to the starting point of the procedure, is outlined. Finally, the effectiveness of the approach is confirmed by an extensive numerical analysis, which also shows the stability of the solution against noise on data.**

***Index Terms*—Antenna radiation patterns, far field, near field.**

I. Introduction

ANTENNA diagnostics from (complex) near-field measurements is a well-established technique at microwave frequencies that is now also becoming increasingly interesting at millimeter frequencies when testing antennas in radioastronomic and radiometric applications [1].

However, various factors make near-field phase measurements more and more inaccurate with increasing frequency. These include: probe-positioning errors (especially along the direction perpendicular to the scanning plane); temperature changes and the mechanical movement of the cables connecting the probe to the receiver; the relative humidity variation during the measurements; and the stability and accuracy of the receiver and transmitter [2].

The use of very sophisticated and, hence, costly measurement equipment is thus obligatory. In particular, the complexity of the measurement facility increases with the working frequency and the dimension of the antenna being tested mainly because of the increasingly stringent requirements on the translation gears (see [2, table 6.10]) that are dictated by the phase-measurement accuracy.

To the best of our knowledge, the only available (amplitude and phase) near-field measurement setup in the millimeter range has a 90-cm $\times$ 90-cm-wide scan area and was employed for the testing of submillimeter-wave astronomy satellite (SWAS) antenna with an aperture of 53 cm $\times$ 68 cm and working at 500 Ghz [3].

In order to overcome the problem of inaccuracy in near-field phase measurements, various near-field far-field transformation approaches have been recently proposed. At present, the most promising techniques are microwave holography and the phase retrieval technique.

Microwave holography [4] is based on Gabor holography [5] (first introduced in electron microscopy) and exploits the measurement of the interference intensity pattern between the antenna under test (AUT) and a transmitted reference wave. The pattern measured is numerically processed to obtain the far field radiated by the AUT.

There are a number of drawbacks to this technique. First of all, to obtain a reasonable scan time, i.e., an acceptable interval between the measurement points, the measurement plane must be sufficiently *far* away from the aperture plane., i.e., testing a 2-m-diameter antenna at 1000 GHz requires a measurement plane which is 15 m away from the antenna. Accordingly, the distance of the measurement surface from the AUT is greater than that required by conventional near-field techniques and this results in a significant increase in the cost of the measurement facility.

In addition, the accuracy of far-field evaluation is closely related to a precise knowledge of the reference antenna since the reference wave must be removed from the measured signal in order to obtain the far-field of the AUT.

Last, the stability of the reference wave must be ensured during the measurement time; this becomes more and more vital as the frequency and the dimensions of the AUT increase.

The second technique, i.e., phase retrieval [6], [7] considers the inverse problem of determining a complex function from amplitude only data and has met with significant interest, not just in near-field far-field transformation techniques [8], [9], but also in antenna metrology and diagnostics [10]–[13].

With this technique, the solution is found as the global minimum of a functional whose unknowns best fit the data. Since the functional is nonquadratic with respect to the unknowns, it can exhibit local minima where the minimization algorithms can be trapped.

Manuscript received July 27, 1998; revised January 7, 1999. This work was supported by Italian MURST.

R. Pierri is with the Dipartimento di Ingegneria dell'Informazione, Seconda Universita' di Napoli, Aversa, 29-I-81031 Italy.

G. D'Elia and F. Soldovieri are with the Dipartimento di Ingegneria Elettronica e delle Telecomunicazioni, Universita' "Federico II" di Napoli, Napoli, 21 I-80125 Italy.

Publisher Item Identifier S 0018-926X(99)04845-0.

In fact, the minimization schemes usually employed are essentially of a "local" type and only allow us to reach the minimum closer to the starting point of the iterative minimization procedure. Accordingly, the solution found can also correspond to a local minimum (false solution) and can be completely different to the true solution. Hence, the local minima problem heavily affects the reliability of the phase retrieval approaches.

The two main classes of algorithms available in literature differ mainly in the choice of the objective functional to be minimized. A first class of phase retrieval algorithms is based on the minimization of the distance between the amplitude of the measured and the reconstructed near-field [6], [9], [14] and handles a highly nonlinear objective functional. The other one considers the distance between the squared amplitude of the measured and the reconstructed near field and, thus, formulates the problem as the inversion of a quadratic operator—a rather simple nonlinearity [7]. As shown in [15], this choice allows better performances of the phase retrieval algorithm with respect to the local minima problem. In addition, it allows us to analyze the local minima problem thoroughly. In particular, the analysis performed in [16] has recognized that the ratio between the amount of independent data and the number of unknowns is the key factor in avoiding the local minima problem.

Thus, in order to ensure the reliability of near-field phase-reconstruction algorithms, the approaches available to date require a knowledge of the amplitude of the near-field over *two measurement surfaces.*

Furthermore, the choice of nonredundant and efficient representations of the field, which exploit all the available *a priori* information, is also crucial in avoiding false solutions.

The need for two scanning surfaces can lead to a more time-consuming measurement procedure with respect to the conventional one, based on the complex near-field measurement, and can require larger anechoic chambers (thus leading to a significant increase in the cost of the overall measurement facility).

However, requiring the smallest possible measurement time is a more and more stringent need for increasing frequency, given the rigorous constraints on the stability of the measurement setup needed to ensure the desired measurement accuracy [2].

A promising approach (at present available only at microwave frequencies) that reduces the scan time, performs thermographic measurements of the near field [17] by means of a resistive sheet that absorbs energy in proportion to the intensity of the incoming field. A thermal picture of the heat pattern on the resistive sheet is taken by means of an infrared imaging camera, which gives the value of the field intensity at each point on the absorbing sheet. This measurement technique makes it possible to overcome the problem of probe position errors and probe correction errors and to perform near-field measurements in a negligible interval of time. The measurement data obtained by using termographic technique have been processed by employing either phase retrieval method [17] or the holographic approach [18]. However, the effectiveness of this technique is limited by the low achievable measurements dynamic range, which, at present, is limited to about 20 dB.

The aim of this paper is to present a new testing technique using only near-field intensities, which makes it possible to overcome the abovementioned drawbacks that are typical of the phase-retrieval-based approaches available up to now.

The technique exploits the squared amplitude of the voltages collected by two different probes simultaneously moving over a *single* scanning surface in near zone. The required scan time is thus equal to that of the conventional complex near-field measurement.

The results of an extensive numerical analysis suggest that the difference between the plane wave spectra of the two probes makes it possible to obtain the required amount of independent squared-amplitude data

Following [7], [16], [19], the presented approach is based on the choice of the *squared amplitude* of the voltages received by the two probes as data of the problem and, thus, involves the inversion of a *quadratic* operator.

The paper is organized as follows. In Section II, the far-field estimation from near-field intensity data is presented for a planar scanning surface. The near-field phase-retrieval problem is recast as the inversion of a quadratic operator and the solution is defined as the global minimum of a quartic functional with respect to the unknowns. The key factors affecting the reliability of the near-field phase recovery approach are analyzed. In Section III, the near-field/far-field transformation procedure is described and its effectiveness and stability are numerically shown.

II. The Formulation of the Problem

Let us consider a planar focusing source, i.e., a source radiating nearly all its power within a bounded angular domain of the visible domain of size $2a$ and $2b$ along the x- and y-axis, respectively, located on the plane $z = 0$, with a y-directed aperture field.

The transverse y component of the near-field over the plane at $z = d$ is expressed [20] as

$$E(x, y, d) = \int_{-\infty}^{\infty} dv \int_{-\infty}^{\infty} \hat{E}(u, v)\, e^{-j(ux+vy+wd)}\, du = T_1(\hat{E}) \tag{1}$$

where $u = \beta \sin\theta \cos\phi$, $v = \beta \sin\theta \sin\phi$, $w = \beta \cos\theta$, $\beta = 2\pi/\lambda$, λ is the wavelength, T_1 is a linear operator [21] relating the plane wave spectrum (PWS) transverse component $\hat{E}(u, v)$ to the near-field transverse component $E(x, y, d)$ and an $e^{j\omega t}$ time dependence has been considered and omitted.

By (1), it follows that if the transverse component of the (complex) near-field $E(x, y, d)$ is known over the whole plane, the PWS can be determined. The far field is then straightforwardly evaluated.

In near-field phaseless technique [7], in order to ensure the reliable determination of the radiation pattern of the AUT, at variance with the conventional (phase and amplitude) measurement technique, a second set of data is required.

The y-component $E(x, y, d_2)$ of the near field over a second scanning plane at $z = d_2$ is related to $\hat{E}(u, v)$ through the linear operator $T_2 = T_1 e^{jw(d-d_2)}$.

It can be seen [7] that when the spacing between the two planes increases, the role of the "defocussing term" $e^{jw(d-d_2)}$ becomes more relevant in making the two sets of the squared amplitude data more "different," with the result that the information content increases.

In this paper, we will obtain the same effect by considering a single plane but two different probes.

In fact, let us consider the case of two different probe antennas with a y-directed aperture field, simultaneously moving over the measurement plane at $z = d$.

The open-circuit voltage received by each probe is expressed by means of an integral involving the source and the probe plane wave spectra [20]. In the case considered here, denoted by $G_1(u, v)$ and $G_2(u, v)$ the y component of the first and second probe PWS, respectively, the received voltages $\mathcal{V}_1$ and $\mathcal{V}_2$ can be expressed as

$$\begin{aligned}\mathcal{V}_i(x, y, d) &= \frac{8\pi^2}{\zeta\beta\nu}\int_{-\infty}^{\infty} dv \int_{-\infty}^{\infty}\left(w - \frac{v^2}{w}\right) \\ &\quad \cdot \hat{E}(u, v) G_i(u, -v)\, e^{-j(ux+vy+wd)}\, du \\ &= \mathcal{T}_i(\hat{E}) \end{aligned} \tag{2}$$

where $i = 1, 2$, ν is a constant with the dimensions of a current, ζ is the free-space characteristic impedance, and $\mathcal{T}_i$ is a linear operator relating the PWS transverse component $\hat{E}(u, v)$ to the output voltage $\mathcal{V}_i$.

According to (2), the linear operators $\mathcal{T}_i$ can be expressed as $\mathcal{T}_i = T_1 G_i(u, -v)(w - v^2/w)$. The difference between the two probe PWS $G_1(u, v)$ and $G_2(u, v)$ ensures the required amount of independent data which, in the approaches available in literature, are obtained by collecting the data over two different scanning surfaces [7].

As stated previously, the problem under consideration involves the determination of the far field radiated by the antenna being tested from the knowledge of the squared amplitude of the voltages received by the two probes, say $M_1^2 = |\mathcal{V}_1|^2$, $M_2^2 = |\mathcal{V}_2|^2$.

Relation (2) leads to the natural choice of $\hat{E}(u, v)$ as the unknown of the problem.

The possibility of introducing a finite-dimensional representation for the PWS $\hat{E}(u, v)$ can be achieved by exploiting the *a priori* information on the AUT.

First, due to the finite extent of the radiating system, $\hat{E}(u, v)$ is a bandlimited function, so that it is amenable to a Shannon sampling series representation involving, in principle, a nonfinite number of samples [22].

Second, we assume the *a priori* information on the direction of the main lobe and the extent of the angular region Ω of the visible domain within which $\hat{E}(u, v)$ is significantly different from zero. Accordingly, $\hat{E}(u, v)$ can be approximated by means of the finite Shannon sampling series involving only the PWS samples $\hat{E}_{nm} = \hat{E}(n\pi/a, m\pi/b)$ falling within Ω [7, see (A1)]. Therefore, for the transverse component of PWS we introduced a finite-dimensional approximation $\tilde{E}(u, v)$ and the samples $\hat{E}_{nm} = \hat{E}(n\pi/a, m\pi/b)$ become the actual unknowns of the problem. Defining the vector $\mathbf{M}^{(2)} = (M_1^2, M_2^2)$ we have

$$\mathbf{M}^{(2)} = (|\mathcal{T}_1\tilde{E}|^2, |\mathcal{T}_2\tilde{E}|^2) = \mathcal{B}(\tilde{E}) \tag{3}$$

so that the problem at hand can be stated as the inversion of the quadratic operator $\mathcal{B}$.

Due to measurement errors and noise, the measured squared amplitude $\tilde{\mathbf{M}}^{(2)} = (\tilde{M}_1^2, \tilde{M}_2^2)$ differ from the ideal ones M_1^2 and M_2^2 and do not necessarily belong to the range of the operator $\mathcal{B}$, so that the existence of a solution $\tilde{E}(u, v)$ satisfying (3) is not ensured. The problem considered here is thus an ill-posed one and will be solved by introducing a "quasi-solution" as the *global* minimum of the functional

$$\begin{aligned}\Phi(\tilde{E}) &= \|\mathcal{B}(\tilde{E}) - \tilde{\mathbf{M}}^{(2)}\|^2 \\ &= \| \, |\mathcal{T}_1\tilde{E}|^2 - \tilde{M}_1^2\|^2 + \| \, |\mathcal{T}_2\tilde{E}|^2 - \tilde{M}_2^2\|^2 \end{aligned} \tag{4}$$

where $\|\cdot\|$ is the quadratic norm (eventually weighted) in the space of data. As the functional (4) is defined over a finite-dimensional space, it admits a minimum by virtue of the Weierstrass theorem [23], so that the problem under investigation has a quasi-solution.

When dealing with a nonlinear inverse problem, the first question to be addressed concerns the uniqueness of the solution. By following the same arguments presented in [24], it is possible to show that the availability of the two sets of data collected by the two different probes makes it possible to ensure the uniqueness of the solution except for an unessential constant phase factor.

In particular, these arguments also allow to understand how the probes must be different. For instance, let us consider the very simple discrete case of probe voltages given by

$$\begin{aligned}\mathcal{V}_1(x) &= \sum_{n=-1}^{1} c_n e^{jnx} \\ \mathcal{V}_2(x) &= \sum_{n=-1}^{1} t_n c_n e^{jnx} \end{aligned} \tag{5}$$

where t_n are the known ratios between the coefficients of the second and first probe, respectively. It can be shown by following the same reasonings presented in [24] that the uniqueness of the solution is ensured when it is possible to solve the linear system of the equations

$$\begin{cases} c_{-1}^* c_0 + c_0^* c_1 = C_1 \\ t_{-1}^* t_0 c_{-1}^* c_0 + t_0^* t_1 c_0^* c_1 = D_1 \end{cases} \tag{6}$$

with respect to the products $c_{-1}^* c_0$ and $c_0^* c_1$, This is allowed provided that $t_{-1}^* t_0 \neq t_0^* t_1$, which gives a measure of how the two probes must be different.

Functional (4) is nonquadratic and the main points concerning its minimization must be addressed. As shown in [16], the local minima problem can be analyzed in a thorough way and the favorable effect of increasing the ratio between the number of independent data and the number of unknowns on the local minima problem can be outlined.

This has been shown in [7], [16] thanks to the definition of a sufficient condition for the lack of local minima in Φ. The

definition of this condition is possible since the functional Φ along a linear variation in the space of the unknowns behaves as a fourth-order polynomial [16]. This condition makes it possible to state that collecting as much independent data as possible plays a key role in overcoming the local minima problem.

This also occurs in the near-field far-field transformation from intensity data, where the increase in the amount of independent data is achieved by means of the addition of a second scanning surface [7].

In the approach presented here, the required number of independent near-field intensity data is obtained by considering a second probe antenna. To ensure an effective increase in the amount of independent data, the PWS of the two probes must be as "different" as possible.

Finally, it must be noted that the accuracy of the far-field estimation also depends on the precision attainable in evaluating $\mathcal{T}_1$ and $\mathcal{T}_2$, which in turn is based on the accuracy in the knowledge of the probes positions and spectra.

III. Numerical Results

The numerical implementation of the algorithm and its effectiveness will be presented in this section. In order to numerically check the algorithm, near-field measured probe-intensity voltages have been numerically simulated.

As far as the evaluation of the operator $\mathcal{B}$ is concerned, it must be noted that the Shannon sampling series representation of $\hat{E}(u, v)$ allows an extensive use of the fast Fourier transform (FFT) algorithm with a resulting efficient and computationally low-cost numerical code.

First, the PWS $\hat{E}(u, v)$ is interpolated from its samples $\hat{E}_{nm}$ within the region Ω by a discrete Fourier transform (DFT), a zero-padding and a subsequent FFT so that the integral in (2) can be accurately evaluated [25]. From the interpolated function $\hat{E}(u, v)$, the voltage spectrum $e^{-jwd}(w - (v^2/w))G(u, -v)\hat{E}(u, v)$ is then evaluated over a uniform grid. The sampling grid is determined by the extent of the measurement domain where the voltages are significantly different from zero, given the Fourier transform relationship between the voltage spectrum and the voltages received by the two probes.

As the PWS $\hat{E}(u, v)$ is significantly different from zero only within Ω, the probe voltage can be approximated by means of a band-limited function, so that the squared amplitude of the voltage is also amenable to a Shannon sampling representation. The samples of the squared amplitude can be computed starting from the voltage spectrum by means of an FFT.

Concerning the minimization of Φ, an iterative procedure based on the Pollak–Ribiere method [26] was applied. In particular, the evaluation of the minimization direction requires the computation of the vector $\underline{\nabla\Phi}$ given by

$$(\underline{\nabla\Phi})_{nm} = \frac{\partial\Phi}{\partial\Re e(\hat{E}_{nm})} + j\,\frac{\partial\Phi}{\partial\Im m(\hat{E}_{nm})} \tag{7}$$

where $\Re e\{\cdot\}$ and $\Im m\{\cdot\}$ denote the real and imaginary part of the corresponding complex quantity, respectively.

As shown in the Appendix, one obtains

$$\begin{aligned}(\underline{\nabla\Phi}) = {} & 4(\mathcal{T}_1\mathcal{P})^{+}[(\mathcal{T}_1\mathcal{P}\underline{c})(|\mathcal{T}_1\mathcal{P}\underline{c}|^2 - \tilde{M}_1^2)] \\ & + 4(\mathcal{T}_2\mathcal{P})^{+}[(\mathcal{T}_2\mathcal{P}\underline{c})(|\mathcal{T}_2\mathcal{P}\underline{c}|^2 - \tilde{M}_2^2)]\end{aligned} \tag{8}$$

where $\underline{c}$ is a complex vector whose components are the samples $\hat{E}(n\pi/a, m\pi/b)$ ordered in an arbitrary way, $\mathcal{P}$ is defined by (A.3), and $+$ stands for the adjoint operation [21]. The evaluation of $\underline{\nabla\Phi}$ can be basically performed by means of the FFT.

The evaluation of the optimal step λ_k, ensuring the maximum decrease of Φ along the updating direction, was performed, in a fast and accurate way by solving a third-degree algebraic equation [8].

A detailed description of the presented technique is given by the flow chart shown in Fig. 1.

The effectiveness of the technique can be improved by introducing suitable weights into the evaluation of Φ in order to enhance the information content of the data corresponding to lower voltage intensities [7], [8], [25]. Since the squared-amplitude distributions can be represented through their samples, a simple but particularly effective choice of the weights consists in the inverse of the corresponding measured intensity voltage samples. Accordingly, the weighted discretized version of the functional Φ is defined as

$$\Psi(\tilde{E}) = \sum_{ij} \frac{(|(\mathcal{T}_1\tilde{E})_{ij}|^2 - \tilde{M}_{1ij}^2)^2}{M_{1ij}^2} + \frac{(|(\mathcal{T}_2\tilde{E})_{ij}|^2 - \tilde{M}_{2ij}^2)^2}{M_{2ij}^2} \tag{9}$$

where $|(\mathcal{T}_1\tilde{E})_{ij}|^2$, $|(\mathcal{T}_2\tilde{E})_{ij}|^2$, M_{1ij}^2, and M_{2ij}^2 are the first and second probe ideal and measured intensity voltage samples, respectively.

The accuracy of the results was evaluated by means of the normalized error defined as

$$\epsilon_M = 10 \times \log\left(\frac{\sum_{ij}(|(\mathcal{T}_1\tilde{E})_{ij}| - \tilde{M}_{1ij})^2}{\sum_{ij} M_{1ij}^2} + \frac{\sum_{ij}(|(\mathcal{T}_2\tilde{E})_{ij}| - \tilde{M}_{2ij})^2}{\sum_{ij} M_{2ij}^2}\right). \tag{10}$$

A square planar source of side $2a = 2b = 10\lambda$ with the aperture field y component given by

$$\begin{aligned}E_{ap}(x, y) = {} & \cos[\pi y/(2a)]\,\exp(-Kx^2)\,\exp(-jK_1x^2) \\ & \cdot \exp(-jK_2y^2)\end{aligned} \tag{11}$$

was considered. The constants K, K_1, and K_2 are such that $|E_{ap}(a, 0)| = -40$ dB and $(K_1a^2) = (K_2a^2) = (\pi/2)$, respectively.

The first probe is given by an E-plane sectorial horn with a 0.8-$\lambda\times$ 5-λ-wide aperture and with the larger side oriented along the y axis. The y component of the probe aperture field

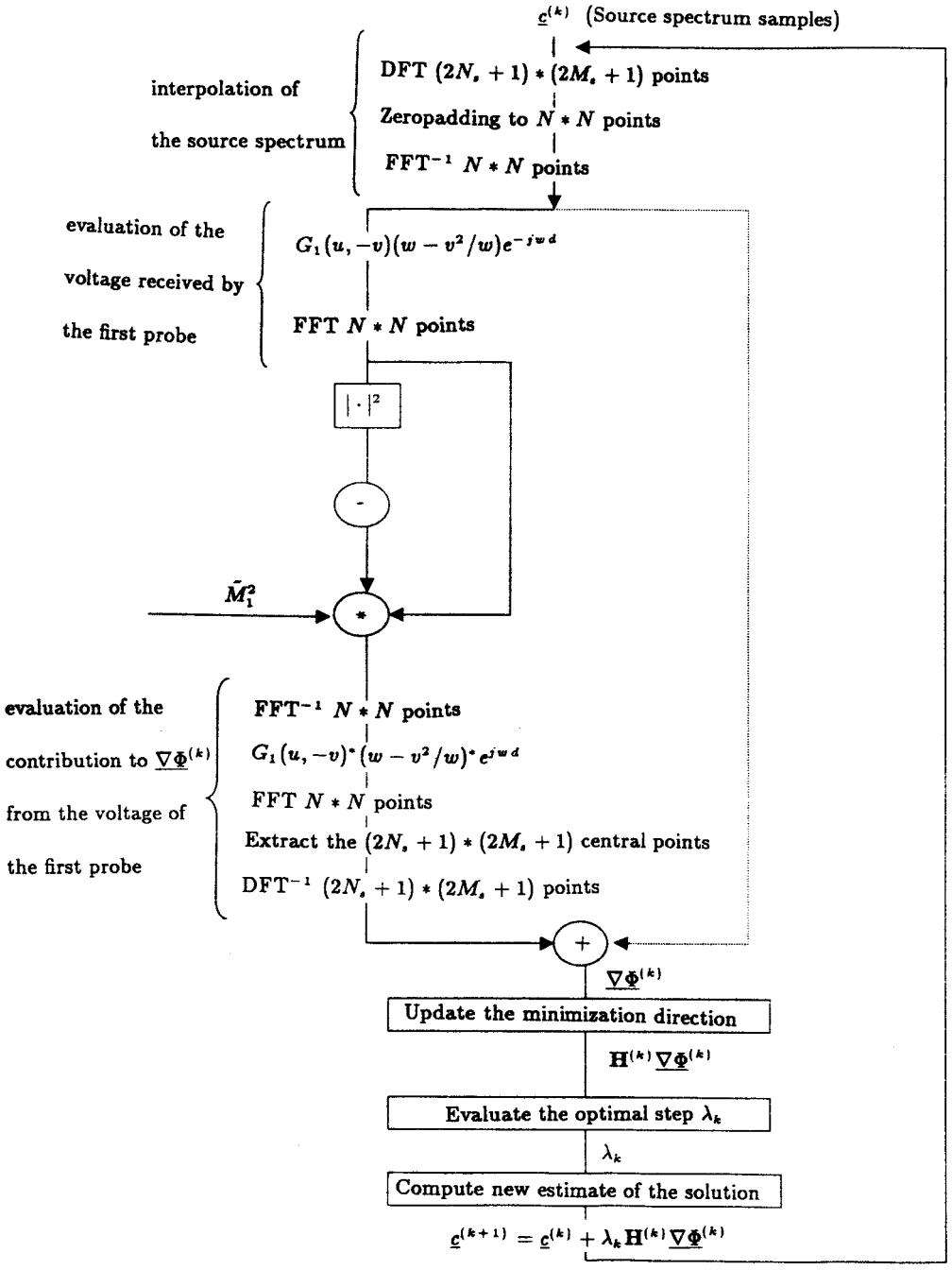

Fig. 1. Flow chart of the solution algorithm: operations along the dashed line referring to the second probe are equal to those on the parallel branch, but with $G_2(u,-v)$ instead of $G_1(u,-v)$.

is given by

$$E_{p1}(x,y)=\cos(\pi x/a')\exp[(-j\beta y^2)/(2R_1)] \tag{12}$$

with $R_1=12\lambda$ and $a'=0.8\lambda$.

The second probe is given by a H-plane sectorial horn with a 5-$\lambda\times$ 0.8-λ-wide aperture and with the larger side oriented along the x axis. The y component of the probe aperture field is given by

$$E_{p2}(x,y)=\cos(\pi x/a'')\exp[(-j\beta x^2)/(2R_2)] \tag{13}$$

with $R_2=12\lambda$ and $a''=5\lambda$.

The two probes are 4λ spaced along a line parallel to the y axis.

The squared amplitude of the voltages received by the probes were simulated on a grid of 128 $\times$ 128 measurement points, $\lambda/4$ spaced between each other on the plane $z=5\lambda$.

Noise-free data were considered first. The samples $\hat{E}_{nm}=\hat{E}(n\pi/5, m\pi/5)$ belonging to the square region Ω of the visible domain of side 0.8β are the unknowns of the problem. A completely *random* set of PWS samples was considered as the starting point of the iterative minimization procedure.

In the early stages of the minimization procedure, only the significant samples of $\tilde{E}(u,v)$ were considered. This makes it possible to perform the beginning of the minimization procedure with an enlarged ratio between the amount of

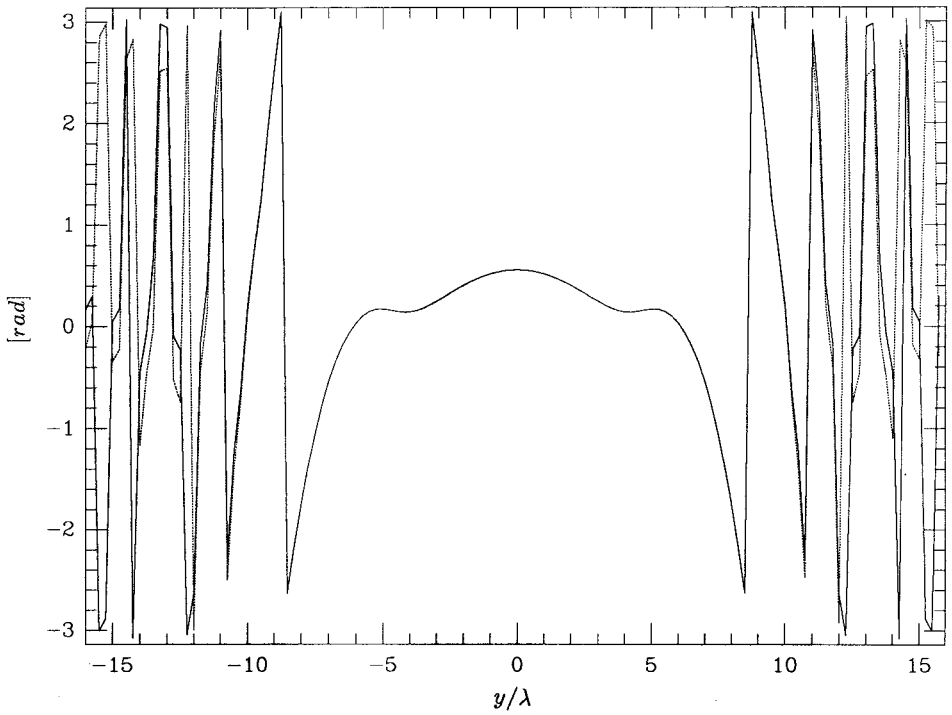

Fig. 2. Comparison between the ideal voltage phase (solid line) and the retrieved phase (dotted line) received by the first probe on the cut line $x = 0$ for the first test case.

independent data and the number of unknowns so that a favorable effect on the local minima is obtained [7]. In fact, an approximated reconstruction of $\tilde{E}(u, v)$ falling within the attraction domain of the global minimum of Φ was obtained.

In particular, at the beginning of the minimization procedure 11×11 samples $\hat{E}_{nm}$ falling within the central region of the visible domain were considered. The minimization of Φ gives an error $\epsilon_M = -42$ dB.

Once the significant samples of $\tilde{E}(u, v)$ were reliably estimated, the solution was improved by gradually increasing the number of the unknowns to be searched for until all the samples falling within Ω are considered. The final estimate of the unknowns corresponds to $\epsilon_M = -47.77$ dB. Finally, the accuracy of the result is increased by introducing the weighted functional Ψ that leads to a normalized error $\epsilon_M = -70.5$ dB.

The exact (solid line) and retrieved (dotted line) phase of the voltage received from the first probe on the cut lines $x = 0$ and $y = 0$, are shown under Figs. 2 and 3, respectively.

The amplitude of the exact (solid line) and estimated (dotted line) PWS $\hat{E}$ on the cut lines $u = 0$ and $v = 0$, are shown in Figs. 4 and 5, respectively.

The sensitivity of the proposed technique with respect to the noise on data was tested by superimposing an additional 5% uniformly distributed noise on the intensity of the voltages of the previous example.

The error obtained by considering just the 11×11 samples $\hat{E}_{nm}$ is $\epsilon_M = -29.2$ dB while the final value of ϵ_M, obtained after the minimization of Ψ and by considering all samples falling within $\times$, is $\epsilon_M = -37.75$ dB.

The exact (solid line) and the retrieved (dotted line) phase of the voltages received by the first probe on the cut lines $x = 0$ and $y = 0$ are shown under Figs. 6 and 7, respectively.

The amplitude of the exact (solid line) and estimated (dotted line) PWS $\hat{E}$ on the cut lines $u = 0$ and $v = 0$ are shown in Figs. 8 and 9, respectively.

IV. Conclusions

A new technique for the antenna diagnostics from near-field intensity data only has been presented.

This technique takes as data of the problem the squared amplitude of the voltages received by *two* different probes over a single planar observation surface in the near-zone of the antenna. The different behavior of the two PWS probes plays a decisive role in obtaining the right amount of data, thus ensuring the reliability of the near-field phase recovery.

The necessity of two scanning surfaces, required by the existing techniques, is overcome, thus obtaining two significant advantages.

First, the size of the anechoic chamber is the same as that required by the conventional near-field measurement techniques based on the measurement of the complex near field.

Second, the measurements made by the two probes can be performed simultaneously so that the measurement time also is equal to that required by conventional near-field measurement techniques. As compared to the available intensity near-field-only techniques, this property leads to very significant advantages when the requirements concerning the stability and the accuracy of the transmitter and receiver are considered.

Although the technique has been presented for a scalar case and planar scanning, it can be easily extended to the vectorial case and/or to different scanning geometries, e.g., cylindrical geometry.

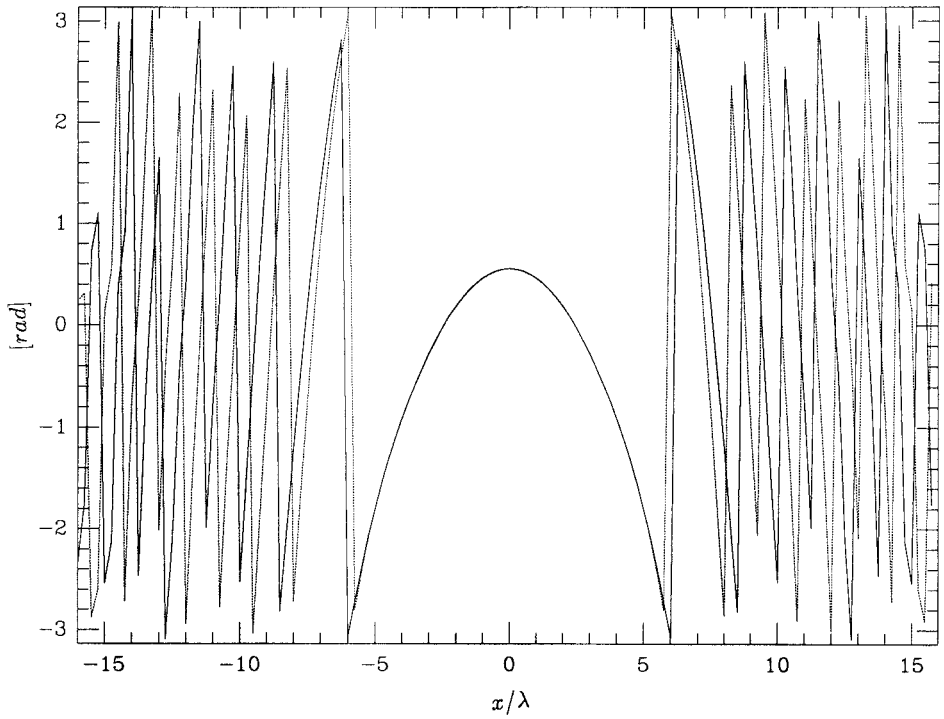

Fig. 3. Comparison between the ideal voltage phase (solid line) and the retrieved phase (dotted line) received by the first probe on the cut line $y = 0$ for the first test case.

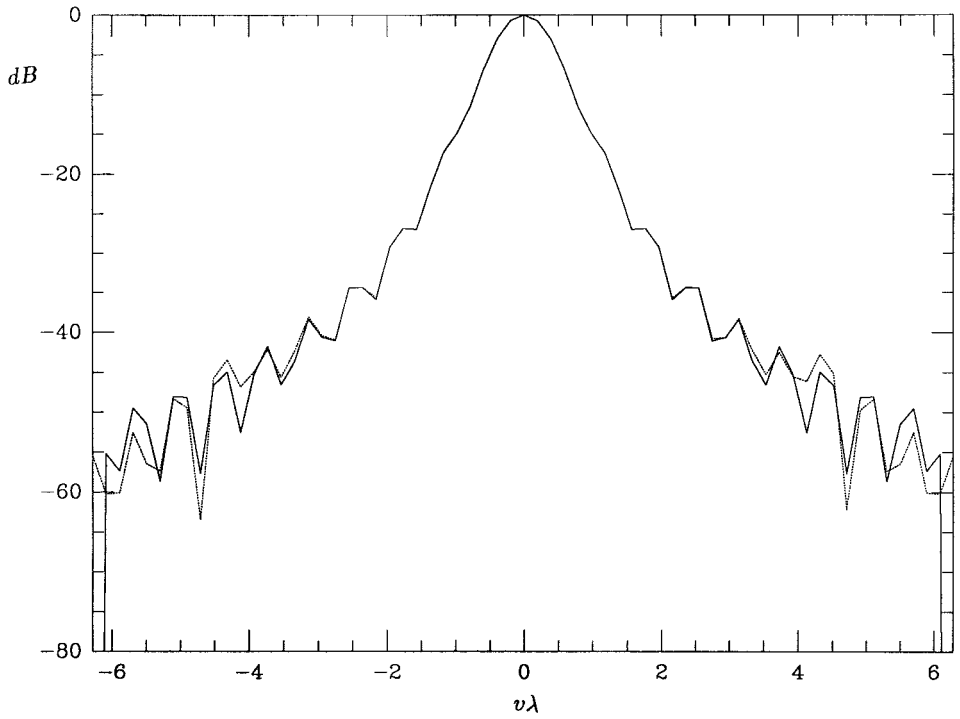

Fig. 4. Comparison between the amplitude of the transverse component of the ideal PWS (solid line) and the estimated PWS (dotted line) on the cut line $u = 0$ for the first test case.

Furthermore, the effectiveness of the approach should be tested also in the case of focusing antennas at millimeter frequencies.

A further possible application of the approach concerns the characterization of the quiet zone of a compact test range from field intensity data only, since the phase measurement becomes inaccurate as the working frequency increases.

In addition, the basic idea of the approach can also be applied to the reflector antenna diagnostics from field intensity data only [13]. This can be made by employing a receiving feed array under different excitation configurations for collecting the two squared-amplitude measurements of the field at feed location. This can allow the two sets of the squared amplitude data to be acquired during a unique rotation of

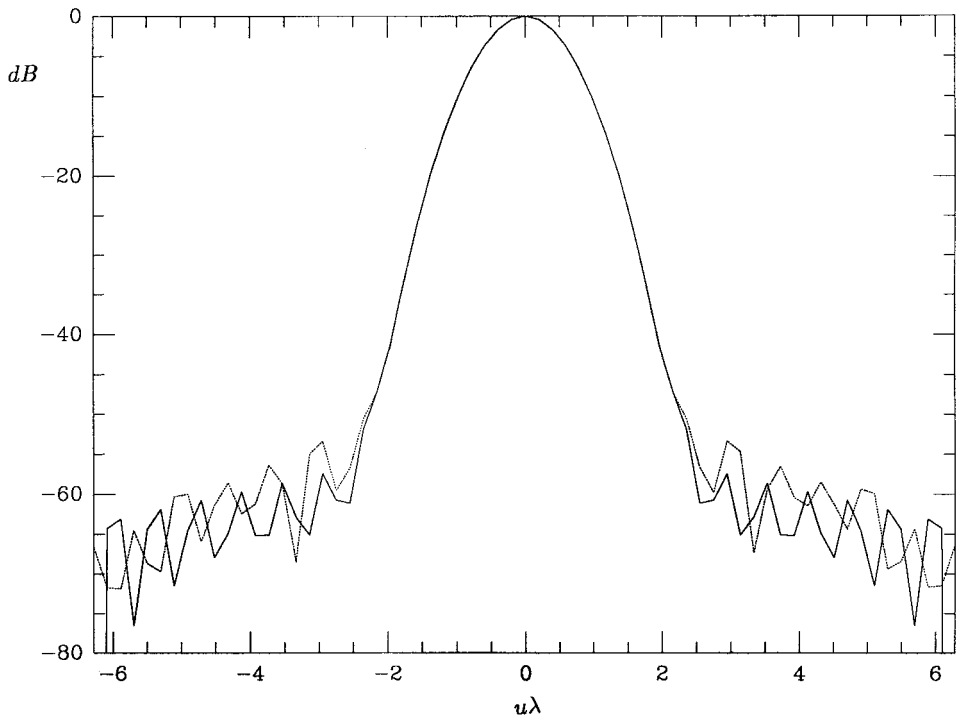

Fig. 5. Comparison between the amplitude of the transverse component of the ideal PWS (solid line) and the estimated PWS (dotted line) on the cut line $v = 0$ for the first test case.

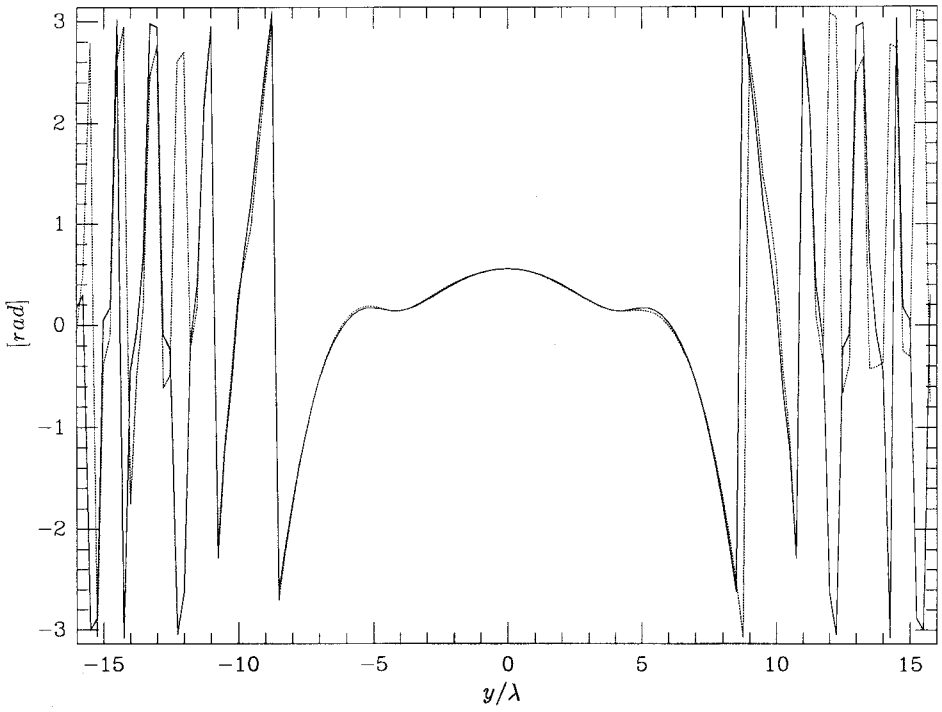

Fig. 6. Comparison between the ideal voltage phase (solid line) and the retrieved phase (dotted line) received by the first probe on the cut line $x = 0$ for the noise-data test case.

the antenna being tested, with a reduced sensitivity of the technique with respect to the instabilities of the signal source and the atmosphere.

APPENDIX

This appendix is devoted to deriving the expression for the vector $\underline{\nabla\Phi}$ given in (8). To this end, it is useful to give some definitions.

First, we recall that the PWS transverse component $\hat{E}(u, v)$ is approximated in a finite-dimensional space according to

$$\tilde{E}(u, v) = \sum_{n=-N_s}^{N_s} \sum_{m=-M_s}^{M_s} \hat{E}(n\pi/a, m\pi/b)\,\mathrm{sinc}(au - n\pi) \cdot \mathrm{sinc}(bv - m\pi) \tag{A.1}$$

where in the summation only the samples falling within Ω must be considered and $\mathrm{sinc}(x) = \sin(x)/x$.

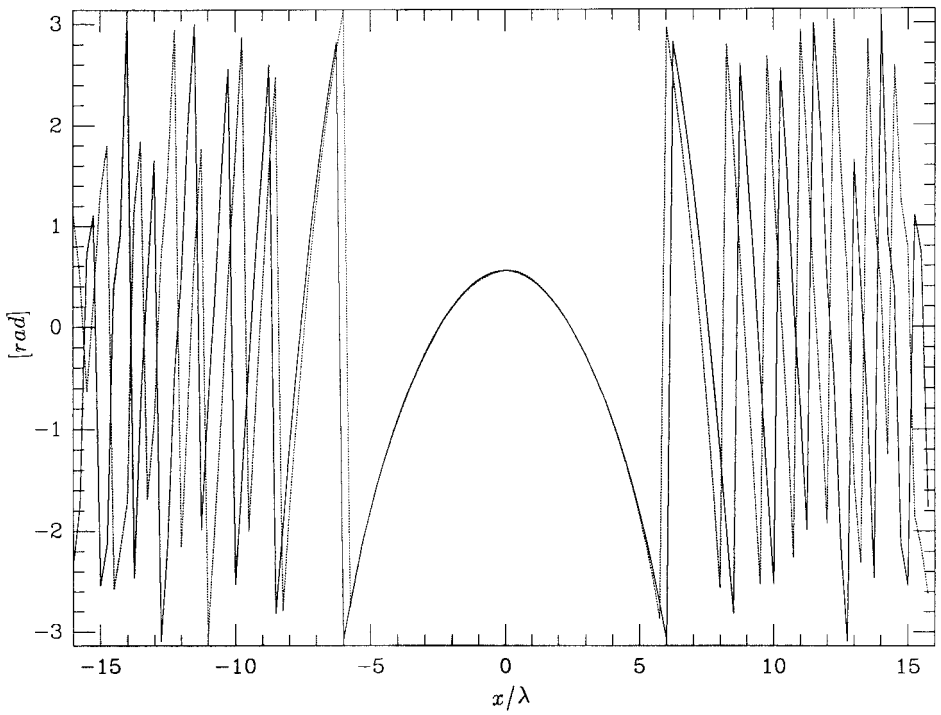

Fig. 7. Comparison between the ideal voltage phase (solid line) and the retrieved phase (dotted line) received by the first probe on the cut line $y = 0$ for the noise-data test case.

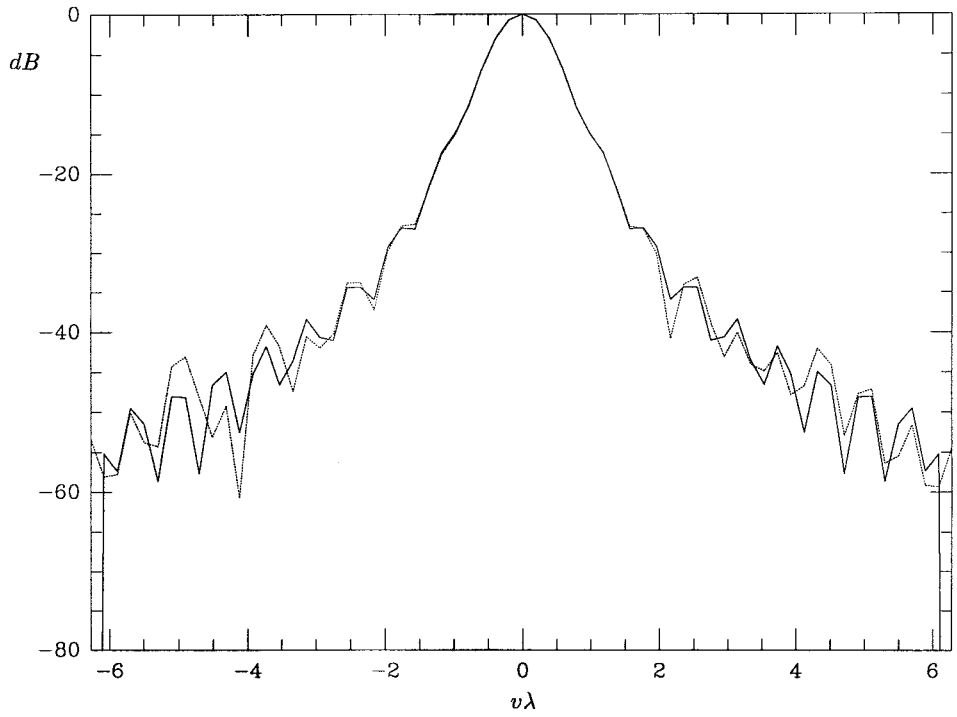

Fig. 8. Comparison between the amplitude of the transverse component of the ideal PWS (solid line) and the estimated PWS (dotted line) on the cut line $u = 0$ for the noise-data test case.

Second, we consider the adjoint $\mathcal{T}_i^+$ of the linear operator $\mathcal{T}_i$, which is given by

$$\begin{aligned}\hat{E}(u, v) &= \mathcal{T}_i^+ \mathcal{V} \\ &= \frac{8\pi^2}{\zeta\beta\nu}\left[\left(w - \frac{v^2}{w}\right) G_i(u, -v)\right]^* \int_{-\infty}^{\infty} dx \int_{-\infty}^{\infty} \\ &\quad \cdot \mathcal{V}(x, y, d)\, e^{j(ux+vy+wd)}\, dy \end{aligned} \tag{A.2}$$

where $*$ stands for the complex conjugate operation.

Third, we define the operator $\mathcal{P}$, which relates the vector $\underline{c}$, whose components are the terms $\hat{E}_{nm}$ with $-N_s \le n \le N_s$ and $-M_s \le m \le M_s$ and are ordered in an arbitrary way to the function $\hat{E}(u, v)$ according to

$$\begin{aligned}\hat{E}(u, v) &= \mathcal{P}\underline{c} \\ &= \sum_{n=-N_s}^{N_s} \sum_{m=-M_s}^{M_s} \hat{E}_{nm} \operatorname{sinc}(au - n\pi) \operatorname{sinc}(bv - m\pi).\end{aligned} \tag{A.3}$$

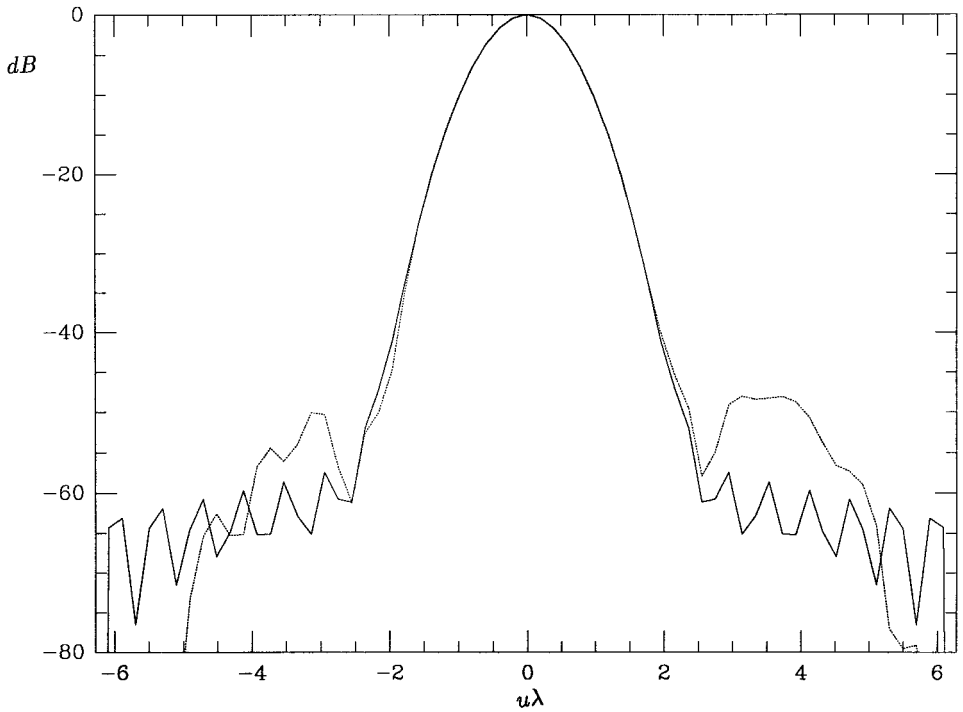

Fig. 9. Comparison between the amplitude of the transverse component of the ideal PWS (solid line) and the estimated PWS (dotted line) on the cut line $v = 0$ for the noise-data test case.

Accordingly, the adjoint operator of $\mathcal{P}$ is defined according to

$$\begin{aligned}\hat{E}_{nm} &= (\mathcal{P}^{+}\tilde{E}(u, v))_{nm} \\ &= \int_{-\infty}^{\infty} du \int_{-\infty}^{\infty} \operatorname{sinc}(au - n\pi) \\ &\quad \cdot \operatorname{sinc}(bv - m\pi)\tilde{E}(u, v)\, dv. \end{aligned} \tag{A.4}$$

Now, by substituting the transverse component of the PWS $\hat{E}$ with its finite-dimensional version (A.1), the voltage $\mathcal{V}_i(x, y, z)$ is given by

$$\begin{aligned}&\mathcal{V}_i(x, y, d) \\ &= \sum_{n=-N_s}^{N_s} \sum_{m=-M_s}^{M_s} \hat{E}(n\pi/a, m\pi/b)\, \frac{8\pi^2}{\zeta\beta\nu} \int_{-\infty}^{\infty} du \int_{-\infty}^{\infty} \\ &\quad \cdot \left(w - \frac{v^2}{w}\right) G_i(u, -v) \operatorname{sinc}(au - n\pi) \\ &\quad \cdot \operatorname{sinc}(bv - m\pi)\, e^{-j(ux+vy+wd)}\, dv \\ &= \mathcal{I}_i \mathcal{P}\underline{c} \end{aligned} \tag{A.5}$$

where $\underline{c}$ is the vector of the samples $\hat{E}(n\pi/a, m\pi/b)$.

In order to compute the vector $\underline{\nabla\Phi}$, we must evaluate the partial derivatives of Φ with respect to the real variables $\Re e\{\hat{E}_{nm}\}$ and $\Im m\{\hat{E}_{nm}\}$. To this end, it is useful first of all to evaluate the partial derivatives of $|\mathcal{I}_i\mathcal{P}\underline{c}|^2$ which, after simple manipulations, are given by

$$\frac{\partial|\mathcal{I}_i\mathcal{P}\underline{c}|^2}{\partial\Re e\{\hat{E}_{nm}\}} = 2\Re e\{(\mathcal{I}_i\mathcal{P}\underline{c})^{*}(\mathcal{I}_i \operatorname{sinc}(au - n\pi)\operatorname{sinc}(bv - m\pi))\} \tag{A.6}$$

and

$$\frac{\partial|\mathcal{I}_i\mathcal{P}\underline{c}|^2}{\partial\Im m\{E_{nm}\}} = 2\Im m\{(\mathcal{I}_i\mathcal{P}\underline{c})^{*}(\mathcal{I}_i \operatorname{sinc}(au - n\pi)\operatorname{sinc}(bv - m\pi))\} \tag{A.7}$$

respectively.

Accordingly, the partial derivative of Φ with respect to $\Re e\{E_{nm}\}$ is evaluated as

$$\begin{aligned}&\frac{\partial\Phi}{\partial\Re e\{E_{nm}\}} \\ &\quad = \langle 2\Re e\{(\mathcal{I}_1\mathcal{P}\underline{c})^{*}(\mathcal{I}_1 \operatorname{sinc}(au - n\pi)\operatorname{sinc}(bv - m\pi))\} \\ &\quad\quad |\mathcal{I}_1\mathcal{P}\underline{c}|^2 - \tilde{M}_1^2\rangle + \langle 2\Re e\{(\mathcal{I}_2\mathcal{P}\underline{c})^{*}(\mathcal{I}_2 \operatorname{sinc}(au - n\pi) \\ &\quad\quad \cdot \operatorname{sinc}(bv - m\pi))\},\, |\mathcal{I}_2\mathcal{P}\underline{c}|^2 - \tilde{M}_2^2\rangle + c.c. \\ &\quad = 4\Re e\{\mathcal{P}^{+}\mathcal{I}_1^{+}[\mathcal{I}_1\mathcal{P}\underline{c}(|\mathcal{I}_1\mathcal{P}\underline{c}|^2 - \tilde{M}_1^2)] \\ &\quad\quad + \mathcal{P}^{+}\mathcal{I}_2^{+}[\mathcal{I}_2\mathcal{P}\underline{c}(|\mathcal{I}_2\mathcal{P}\underline{c}|^2 - \tilde{M}_2^2)]\} \end{aligned} \tag{A.8}$$

where $\langle\cdot, \cdot\rangle$ means the scalar product and *c.c.* denotes the complex conjugate of the addition of the two previous terms.

In a similar way, it is possible to evaluate the partial derivative of Φ with respect to $\Im m\{\hat{E}_{nm}\}$, which is given by

$$\begin{aligned}\frac{\partial\Phi}{\partial\Im m\{\hat{E}_{nm}\}} &= 4\Im m\{\mathcal{P}^{+}\mathcal{I}_1^{+}[\mathcal{I}_1\mathcal{P}\underline{c}(|\mathcal{I}_1\mathcal{P}\underline{c}|^2 - \tilde{M}_1^2)] \\ &\quad + \mathcal{P}^{+}\mathcal{I}_2^{+}[\mathcal{I}_2\mathcal{P}\underline{c}(|\mathcal{I}_2\mathcal{P}\underline{c}|^2 - \tilde{M}_2^2]\}. \end{aligned} \tag{A.9}$$

Finally, the vector (7) given by

$$(\underline{\nabla\Phi})_{nm} = \frac{\partial\Phi}{\partial\Re e(\hat{E}_{nm})} + j\,\frac{\partial\Phi}{\partial\Im m(\hat{E}_{nm})}$$

can be computed as

$$\begin{aligned}(\underline{\nabla\Phi}) &= 4(\mathcal{I}_1\mathcal{P})^{+}[(\mathcal{I}_1\mathcal{P}\underline{c})(|\mathcal{I}_1\mathcal{P}\underline{c}|^2 - \tilde{M}_1^2)] \\ &\quad + 4(\mathcal{I}_2\mathcal{P})^{+}[(\mathcal{I}_2\mathcal{P}\underline{c})(|\mathcal{I}_2\mathcal{P}\underline{c}|^2 - \tilde{M}_2^2)]. \end{aligned} \tag{A.10}$$

REFERENCES

[1] J. Ala-Laurinaho, P. R. Foster, G. J. Junkin, T. Hirvonen, A. Letho, D. H. Martin, A. D. Olver, R. Padman, C. Parini, A. V. Raisanen, T. Sehm, J. Tuovinen, and R. J. Wylde, "Comparison of antenna measurement techniques for 200–1500 GHz," in *Proc. 20th ESTEC Antenna Workshop Millimeter Wave Antenna Technol. Antenna Measurements*, Noordwijk, The Netherlands, June 1997, pp. 345–351.

[2] P. R. Foster, D. Martin, C. Parini, A. Raisanen, J. Ala-Laurinhao, T. Hirvonen, A. Letho, T. Sehm, J. Tuovinen, F. Jensen, and K. Pontoppidan, "MMWave antenna testing techniques—Phase 2," MAAS Rep. 304, no. 2, prepared for ESTEC under contract no. 11 641/95/NL/PB(SC), Dec. 1996.

[3] N. Erickson and V. Tolls, "Near-field measurements of the submillimeter wave astronomy satellite antenna," in *Proc. 20th ESTEC Antenna Workshop Millimeter Wave Antenna Technol. Antenna Measurements*, Noordwijk, The Netherlands, June 1997, pp. 313–319.

[4] G. Junkin, J. C. Bennet, and T. Huang, "Holographic near-field/far-field for therahertz antenna testing," in *Proc. 19th Antenna Measurement Tech. Assoc. Meet. Symp.*, Boston, MA, Nov. 1997, pp. 419–423.

[5] D. Gabor, "Microscopy by reconstructed wavefronts," in *Proc. Royal Soc.*, London, U.K., vol. A, no. 197, pp. 454–487, 1949.

[6] O. M. Bucci, G. D'Elia, G. Leone, and R. Pierri, "Far-field pattern determination from the near-field amplitude on two surfaces," *IEEE Trans. Antennas Propagat.*, vol. 38, pp. 1772–1779, Nov. 1990.

[7] T. Isernia, G. Leone, and R. Pierri, "Radiation pattern evaluation from near-field intensities on planes," *IEEE Trans. Antennas Propagat.*, vol. 44, pp. 701–710, May 1996.

[8] T. Isernia, G. Leone, R. and Pierri, "A new approach to antenna testing from near-field phaseless data: The cylindrical scanning," *Proc. Inst. Elect. Eng.*, vol. 139, pt. H, pp. 363–368, Aug. 1992.

[9] Y. Rahmat-Samii and R. G. Yaccarino, "Microwave antenna imaging, diagnostics, and phaseless reconstruction," *Int. J. Imaging Syst. Technol.*, vol. 8, no. 4, pp. 396–406, 1997.

[10] J. E. McCormack, G. Junkin, and A. P. Anderson," Microwave metrology of reflector antennas from a single amplitude," *Proc. Inst. Elect. Eng.*, vol. 137, pt. H, pp. 276–284, Oct. 1990.

[11] O. M Bucci, G. D'Elia, and G. Romito, "Reflector distorsions diagnosis from far-field amplitude pattern," *IEEE Trans. Antennas Propagat.*, vol. 43, pp. 1217–1225, Nov. 1995.

[12] D. Morris, "Simulated annealing applied to Misell algorithm for phase retrieval," *Proc. Inst. Elect. Eng.*, vol. 143, pt. H, no. 4, pp. 298–303, Aug. 1996.

[13] G. Leone and R. Pierri, "Reflector antenna diagnosis from phaseless data," *IEEE Trans. Antennas Propagat.*, vol. 45, pp. 1236–1244, Aug. 1997.

[14] G. Junkin, A. P. Anderson, C. A. E. Rizzo, W. J. Hall, C. J. Prior, and C. Parini, "Near-field/ far-field phase retrieval measurement of a prototype of the microwave sounding unit antenna AMSU-b at 94 GHz," in *Proc. Eur. Space Res. Technol. Ctr. (ESTEC) Conf. Millimeter Wave Technol. Applicat.*, Noordwijk, The Netherlands, 1995.

[15] G. Leone, R. Pierri, and F. Soldovieri, "On the performances of two algorithms in phaseless antenna measurements," in *Proc. 10th Int. Conf. Antennas Propagat. (ICAP)*, Edinburgh, Scotland, Apr. 1997, pp. 1/136–1/141.

[16] T. Isernia, G. Leone, R. Pierri, and F. Soldovieri, "On the local minima in phase reconstruction algorithms," *Radio Sci.*, vol. 31, pp. 1887–1899, Nov./Dec. 1996.

[17] J. E. Will, J. D. Norgard, R. M. Sega, M. Seifert, A. Pesta, J. Cleary, C. Stubenrauch, and K. MacReynolds, "Antenna near-field phase data from infrared thermograms by Fourier iterative plane-to-plane techniques," in *Proc. 18th Antenna Meas. Tech. Assoc. Meet. Symp.*, Seattle, WA, Oct. 1996, pp. 198–203.

[18] C. F. Stubenrauch, K. MacReynolds, J. E. Will, J. D. Norgard, M. Seifert, and R. H. Cormack, "Microwave antenna far-field patterns determined from infrared holograms," in *Proc. 19th Antenna Meas. Tech. Assoc. Meet. Symp.*, Boston, MA, Nov. 1997, pp. 125–130.

[19] T. Isernia, G. Leone, and R. Pierri, "Phase retrieval of radiated fields," *Inverse Problems*, vol. 11, pp. 183–203, 1995.

[20] D. T. Paris, W. M. Leach Jr., and E. B. Joy, "Basic theory of probe-compensated near-field measurements," *IEEE Trans. Antennas Propagat.*, vol. AP-26, pp. 373–379, May 1978.

[21] A. E. Taylor and D. Kay, *Introduction to Functional Analysis.* Malobar FL: Krieger, 1980.

[22] A. D. Yaghjian, "An overview of near-field antenna measurements," *IEEE Trans. Antennas Propagat.*, vol. AP-34, pp. 30–45, Jan. 1986.

[23] G. F. Simmons, *Introduction to Topology and Modern Analysis.* Singapore: McGraw-Hill, 1963.

[24] T. Isernia, G. Leone, and R. Pierri,"A quadratic inverse problem: the phase retrieval," in *Inverse Methods in Action*, P. C. Sabatier, Ed. Berlin, Germany: Springer-Verlag, 1990.

[25] ———, "Numerical and experimental validation of a phaseless planar near-field technique," *J. Elect. Waves Appl.*, vol. 9, pp. 267–284, 1995.

[26] D. Luenberger, *Linear and Nonlinear Programming.* Reading, MA: Addison-Wesley, 1987.

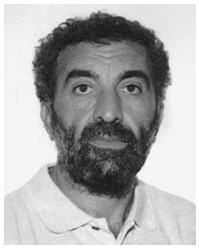

Rocco Pierri was born and educated in Italy. He received the Laurea degree (*summa cum laude*) in electronic engineering from the University of Naples "Federico II," in 1995.

From 1976 to 1990, he worked at the University of Naples as a National Research Council (CNR) Research Fellow, Lecturer, Assistant Professor, and Associate Professor in electronic engineering. Since 1993, he has been a Professor of electronic engineering (electromagnetic waves and applications) at the Second University of Naples. He has contributed in these fields with a relevant number of journal papers. His main scientific interests are antennas, phase retrieval, inverse problems subsurface imaging.

Mr. Pierri is currently organizing and chairing a number of scientific sessions on nonlinear inversion. He is chairman of a research group on inverse scattering subsurface imaging. He is chairman of the Second University of Naples' Ph.D. Committee.

Giuseppe D'Elia, for a photograph and biography, see p. 1225 of the November 1995 issue of this TRANSACTIONS.

Francesco Soldovieri received the B.S. degree from the University of Salerno, Italy, in 1992, and the Ph.D. degree from the University of Naples, Italy, in 1996, both in electronic engineering.

In 1993, he joined the Electromagnetic Research Group, University of Naples "Federico II," Italy. Since 1998 he has held a Postdoctoral Fellowship at the University of Naples. His main scientific interests are antenna measurements, phase retrieval, inverse problems, and antenna synthesis.